Analysis and Optimization of Current Injection Method for Mitigating the Current Ripple of MMC-BESS

Yongzheng Yu, Xiaolei Cheng, Junfang Hao, Xiaotian Yuan, *Member, IEEE*, Qiufeng Shang, and Ying Yang, *Member, IEEE*

***Abstract*—Due to the inherent operational property, the modular multilevel converter battery energy storage system (MMC-BESS) exists battery current ripple issue, which will inevitably affect the battery life and increase the conduction loss. To address this issue, this article investigates the current injection method for mitigating the battery current ripple of MMC-BESS. To analyze the mechanism of current ripple in submodules, the current deviation optimization problem is converted into the energy deviation optimization problem. The effect of the reactor and the battery module is considered to obtain the accurate analytical expression of battery current and capacitor voltage deviation for optimizing the current injection value. Furthermore, the quantitative analysis of factors affecting the battery current ripple is conducted for parameter optimization. The experiment results verify the correctness of the proposed energy-based analysis method as well as the ability of the optimized current injection method to mitigate the battery current ripple.**

***Index Terms*—Current injection method, current ripple suppression, energy deviation, modular multilevel converter battery energy storage system (MMC-BESS).**

I. Introduction

With the development of battery technology, the battery energy storage system (BESS) stands out by the merits of efficiency, flexibility, and low cost [1]. In addition, for the purpose of improving the stability of power systems with a high proportion of renewable energy, the grid-forming control strategies for the BESS are proposed to mimic the similar functions of synchronous generator providing the damping and inertial support for the grid [2], [3]. In practical application, the BESS usually utilizes the power conversion system for energy conversion and adopts power convert like two-level or three-level converter [4]. These topologies are easy to implement but have low voltage level and small capacity, which cannot provide enough strong support for the large power system applications.

Compared to two-level converter, the high voltage level energy storage topology has the advantage of high reliability and faster response speed. It does not need the step-up transformers to connect the network. The high voltage level topologies of BESS with large capacity are therefore proposed, which can be typically divided into cascaded H-bridge BESS (CHB-BESS) [5], [6], [7] and modular multilevel converter BESS (MMC-BESS) [8], [9], [10]. Compared to the CHB-BESS, the MMC-BESS has high transform efficiency, larger single machine capacity, and low control complexity, which can easily control the unbalanced state of charge (SOC) of batteries.

However, based on the operation characteristics of MMC-BESS, the battery module in submodule will suffer from 50 Hz and 100 Hz current ripple, which will lead to the decrease of the calendar life of battery, higher conduction loss, and limit the operation range of BESS [11], [12], [13]. One easy approach is to place the passive filter to mitigate the current ripple [14]. However, this scheme requires large inductance, which will further increase the system investment costs for the practical applications, adversely affecting the dynamic response of the system. To effectively mitigate the battery current ripple with lower costs, the combination of the passive filter and the active control strategies of power switches is necessary.

A possible active control strategy to mitigate the submodule battery current ripple is to inject harmonic voltage into arm's output voltage or to inject harmonic current into arm current. The zero-sequence third-order harmonic voltage injection is proposed in MMC application, achieving the target of mitigating the voltage ripple by increasing the modulation index during system dynamics [15]. To reduce the fundamental and second-frequency voltage oscillations in the submodule capacitor, instead of employing a second-order harmonic suppression controller to completely suppress the arm circulating current, the second-order negative-sequence current injection method is adopted to set the circulating current to a specified value [16], [17]. However,

Received 9 July 2024; revised 30 October 2024 and 26 December 2024; accepted 8 May 2025. Date of publication 19 May 2025; date of current version 30 June 2025. This work was supported by the National Key Research and Development Program of China (2023YFB2408200). Recommended for publication by Associate Editor D. Dong. *(Corresponding author: Ying Yang.)*

Yongzheng Yu and Qiufeng Shang are with the Department of Electronic and Communication Engineering, North China Electric Power University, Baoding 071003, China (e-mail: 220222215050@ncepu.edu.cn; baodingshan-g@ncepu.edu.cn).

Xiaolei Cheng and Junfang Hao are with the Xuji Group Corporation, Xuchang 461000, China (e-mail: chengxiaolei@xj.cee-group.cn; haojunfang-@xj.cee-group.cn).

Xiaotian Yuan is with the Contemporary Amperex Future Energy Research Institute, Shanghai 201100, China, also with the School of Electrical Engineering, Xi'an Jiaotong University Xi'an 710049, China, and also with the School of Electrical and Electronic Engineering, Nanyang Technological University, Singapore 639798 (e-mail: yxt2013@stu.xjtu.edu.cn).

Ying Yang is with the Department of Electrical Engineering, Tsinghua University, Beijing 100084, China (e-mail: yingyang@tsinghua.edu.cn).

Color versions of one or more figures in this article are available at https://doi.org/10.1109/TPEL.2025.3569600.

Digital Object Identifier 10.1109/TPEL.2025.3569600

due to the uncertainty of parameters and operating states of different topologies, the above methods are not universal and may not have the best performance in the MMC-BESS application. Since the main frequency component of the capacitor voltage ripple in CHB-BESS is the second-order harmonic, the current injection method can be used to completely suppress the second-order harmonic voltage oscillation, converting the second-order harmonic to the fourth harmonic, which is easier to be filtered by passive elements [18]. However, the primary frequency component of the submodule battery current ripple is fundamental, possessing a lower harmonic order relative to that of CHB-BESS, which requires injecting greater current into arm circulating current to completely suppress the second-order battery current ripple. Therefore, to prevent excessive current injection into the arm current in MMC-BESS, the preferred current injection method involves concurrent mitigation of both the fundamental and second-order harmonic components, thereby achieving an optimized suppression effect on the peak-to-peak deviation of the battery current ripple. In [19], an analytical expression of capacitor energy ripple is obtained to optimize the current injection method based on the proportional relationship between the deviation of arm energy and capacitor voltage. But in the MMC-BESS application, this proportional relationship does not exist due to the effect of the reactor and the battery module and therefore affects the correctness of the analytical expression. Thus, investigating the impact of the reactor and battery module is necessary to accurately evaluate the deviation of the battery current and capacitor voltage in order to optimize the current injection method.

In this article, the relationship between the arm energy component, battery current, and capacitor voltage is established, and the battery current deviation optimization problem is converted to the energy optimization problem, which also simplifies the analysis of battery current and capacitor voltage ripple. The current injection method is optimized based on the analytical expression of battery current deviation and the positive factors in mitigating battery current ripple are also investigated. The main contributions of this article are listed as follows.

1) Establishing the relationship between the arm energy component, the battery current and the capacitor voltage. This converts the analysis object from the current and voltage to the energy, obtaining the analytical expression of the current and voltage deviation.
2) Utilizing the synchronous reference frame method, the relationship between injected current, grid current, and arm energy is built, simplifying the quantitative analysis of the battery current deviation.
3) Investigating the impact of the reactor, battery module and operating parameters on the current and voltage ripple and the variation of the current deviation before and after injecting current.

The rest of this article is organized as follows. Section II analyzes the MMC-BESS from the perspective of arm energy. Section III investigates the relationship between the capacitor voltage, battery current, and arm energy and proposes the current injection method optimization. Section IV analyzes the effect of ac-side output power, battery output power, and the difference before and after adopting the current injection method. In Section V, the experiment result validates the analysis method, and verifies the effectiveness of the proposed method. Finally, Section VI concludes this article.

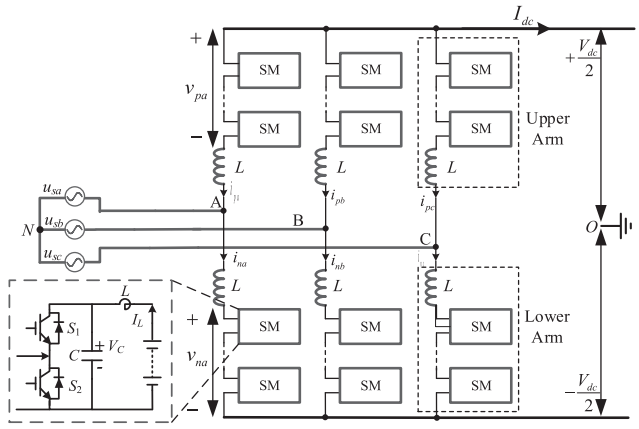

Fig. 1. Structure of MMC-BESS.

II. MMC-BESS From the Perspective of Energy

A. Topology and Power Flow

Fig. 1 depicts the topology of MMC-BESS. Each phase consists of positive and negative arms. Each arm is composed of N submodules. The half-bridge submodule contains two power switches, one capacitor, one reactor, and the battery module.

The power equation between the ac-side of MMC-BESS, dc-side of MMC-BESS, and the battery modules is expressed as follows:

$$P_{\rm ac} + P_{\rm dc} + P_{\rm bat} = 0 \tag{1}$$

where $P_{\rm ac}$, $P_{\rm dc}$, and $P_{\rm bat}$ are the power of the ac-side, dc-side, and battery modules, respectively. This equation indicates that the output power of MMC-BESS can be controlled by any two of the three ports. In the half-bridge submodule, the control of the ac-side output power and the dc-side output power is achieved by the active control of the power switches S_1 and S_2. Since the ac-side and the dc-side output power are controlled, the battery output power is also controlled.

Regardless of the difference in submodule type, as the battery output power and the ac-side output power are the same, the frequency component in the arm voltage and the arm current are the same. The positive and negative arm current and voltage equations in phase j ($j = a, b, c$) are defined as the following equation:

$$\begin{aligned} i_{p,j} &= \frac{I_{\rm dc}}{3} - \frac{I_g}{2}\cos(\omega t + \delta_j + \theta_1) \\ i_{n,j} &= \frac{I_{\rm dc}}{3} + \frac{I_g}{2}\cos(\omega t + \delta_j + \theta_1) \end{aligned} \tag{2}$$

$$\begin{aligned} v_{p,j} &= \frac{V_{\rm dc}}{2} - V_g\cos(\omega t + \delta_j) \\ v_{n,j} &= \frac{V_{\rm dc}}{2} + V_g\cos(\omega t + \delta_j) \end{aligned} \tag{3}$$

where ω is the fundamental frequency, δ_j ($\delta_a = 0$, $\delta_b = -2\pi/3$, $\delta_c = +2\pi/3$), and θ_1 is the phase displacement angle. $I_{\rm dc}$ and $V_{\rm dc}$ are the current and voltage of the dc bus line. I_g and V_g are the amplitudes of the output current and voltage.

From (2) and (3), the full expression of the ac component of the arm energy can be obtained, and the positive arm of phase j is taken as an example of illustration:

$$E_{p,j} = -\frac{V_{\rm dc} I_g \sin(\omega t + \delta_j + \theta_1)}{4\omega} - \frac{mV_{\rm dc} I_{\rm dc}}{6\omega}\sin(\omega t + \delta_j) + \frac{mV_{\rm dc} I_g}{16\omega}\sin(2\omega t + 2\delta_j + \theta_1). \tag{4}$$

According to (4), it can be concluded that the frequency component of the energy ripple consists of the fundamental and second-order harmonic.

B. Current Injection Method

Due to the quadratic relationship between the deviation of the capacitor voltage and arm energy in MMC, mitigating capacitor voltage ripple is achieved by counteracting the arm energy ripple [20]. In MMC-BESS, a similar methodology can be used to mitigate the current and voltage ripple.

To maximize the mitigating effect of the arm energy, the injected current is chosen to be the second-order harmonic in the negative sequence and injected into the circulating current to not affect the output of active and reactive power. The expression of the injected current can be defined as

$$i_{{\rm z},j} = I_z \cos(2\omega t - \delta_j + \theta_2) \tag{5}$$

where θ_2 is the phase angle of the injected current relative to the grid voltage phase angle. The energy component produced by injecting current is calculated as follows:

$$E_{{\rm z},j} = \int v_{p,j} i_{{\rm z},j}{\rm d}t = -\frac{mV_{\rm dc} I_z}{4\omega}\sin(\omega t - 2\delta_j + \theta_2) + \frac{V_{\rm dc} I_z \sin(2\omega t - \delta_j + \theta_2)}{4\omega} - \frac{mV_{\rm dc} I_z}{12\omega}\sin(3\omega t + \theta_2) \tag{6}$$

where the third harmonic is small enough to be neglected. According to (6), it can be concluded that the injected current will produce the fundamental and second-order harmonic component, which can be used to counteract the energy ripple produced by the origin arm voltage and current.

C. Simplification Method

It can be observed from (2) and (3) that the fundamental voltage and current components of the upper and lower arm are opposite, which means the odd-order components of energy expression are opposite phases in the upper and lower arm, while the even-order components of energy expression are the same phase in both arms. Therefore, adding and subtracting the upper and lower arm energy can be used to extract the fundamental and second-frequency components. This method can be mathematically defined as follows:

$$E_{1\omega} = \frac{E_{p,j} - E_{n,j}}{2}, E_{2\omega} = \frac{E_{p,j} + E_{n,j}}{2}. \tag{7}$$

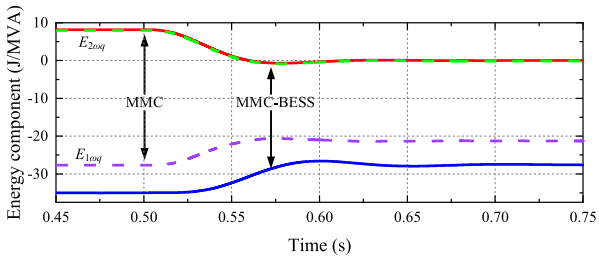

Fig. 2. Comparison of energy component between MMC and MMC-BESS.

To decouple the effect between the active power and the reactive power, as well as simplify the analysis of the relationship between the amplitude of sinusoidal quantities like arm energy, grid current, and injected current, the Park's transformation is adopted in arm energy. The d-axis and q-axis of the fundamental and second frequency component of arm energy can be expressed as follows:

$$E_{2\omega d} = \frac{V_{\rm dc}}{4\omega} I_{zq} + \frac{mV_{\rm dc}}{16\omega} I_{gq},\ E_{2\omega q} = -\frac{V_{\rm dc}}{4\omega} I_{zd} - \frac{mV_{\rm dc}}{16\omega} I_{gd} \tag{8}$$

$$E_{1\omega d} = -\frac{V_{\rm dc}}{4\omega} I_{gq} - \frac{mV_{\rm dc}}{4\omega} I_{zq},$$
$$E_{1\omega q} = \frac{V_{\rm dc}}{4\omega} I_{gd} + \frac{mV_{\rm dc} I_{\rm dc}}{2\omega} + \frac{mV_{\rm dc}}{4\omega} I_{zd} \tag{9}$$

where $E_{1\omega d}$, $E_{1\omega q}$, $E_{2\omega d}$, and $E_{2\omega q}$ are the d-axis and q-axis components of the fundamental frequency and the second harmonic component of energy. I_{zd}, I_{zq}, I_{gd}, and I_{gq} are the d-axis and q-axis component of injected current and grid current, which can be expressed as

$$I_{gd} = I_g \cos(\theta_1), \quad I_{gq} = I_g \sin(\theta_1) \tag{10}$$

$$I_{zd} = I_z \cos(\theta_2), \quad I_{zq} = I_z \sin(\theta_2). \tag{11}$$

Through the above transformation on arm energy, the active and reactive components of the arm energy are separated into d-axis and q-axis components, respectively, which simplifies the analysis of the different factors affecting current and voltage ripple. Besides, it is obvious from (9) that only the expression of $E_{2\omega q}$ contains the $I_{\rm dc}$ value, which varies under different battery output power conditions. According to (1), the relationship between the dc component of the arm current and the battery output power can be derived as

$$I_{\rm dc} = -\frac{3mI_g}{4}\cos(\theta_1) - \frac{P_{\rm bat}}{V_{\rm dc}}. \tag{12}$$

It can be observed that the relationship between the battery output power and the $I_{\rm dc}$ value is linear. The comparison of the energy component between MMC and MMC-BESS is shown in Fig. 2.

In Fig. 2, the solid line and dash line respectively represent MMC-BESS application, in which the battery output power is rated, and the MMC application, which is equal to zero battery output power in the MMC-BESS application according to (12). It can be concluded that before and after injecting current, the amplitude of the second harmonic energy $E_{2\omega q}$ is the same in

both conditions, while the amplitude of the fundamental component in MMC-BESS is larger than that of MMC. Therefore, in MMC-BESS, the battery output power should be considered as an important factor affecting the battery current and the capacitor voltage ripple.

Moreover, due to the difference in the submodule topology between the MMC and the MMC-BESS, the relationship between the arm energy and the current deviation is unclear in the MMC-BESS application. Hence, the following section will investigate the relationship between the arm energy and the current deviation, analyze the effect of the reactor and the battery module, and propose a corresponding optimized current injection method.

III. Injection Current Optimization

A. Relationship Between Current Deviation and Energy Deviation

The conventional analysis method of the capacitor voltage deviation is applicable to the MMC application, which assumes that the arm energy equals to the sum energy of the submodule capacitors in one arm [20]. Since the capacitor energy is proportional to the square of the capacitor voltage, the maximum value of the arm energy is at the same phase of the maximum value of the submodule capacitor voltage, and the minimum value of the arm energy and capacitor voltage is similarly in the same phase. The expression of the maximum and minimum value of the arm energy and the capacitor voltage can be expressed as

$$\begin{cases} V_{\max} = V_{\text{rated}} + \Delta V/2 \\ V_{\min} = V_{\text{rated}} - \Delta V/2 \\ E_{\max} = E_{\text{rated}} + \Delta E/2 = CV_{\max}^{2/2} \\ E_{\min} = E_{\text{rated}} - \Delta E/2 = CV_{\min}^{2/2} \end{cases} \tag{13}$$

where $V_{\max}$, $E_{\max}$, $V_{\min}$, $E_{\min}$, V_{rated}, E_{rated}, ΔV, and ΔE are the maximum, minimum, rated value, and deviation of the capacitor voltage and arm energy. When the capacitor voltage is maximal or minimal, the arm energy also reaches peak value $E_{\max}$ or $E_{\min}$. Through subtracting the maximum $E_{\max}$ to minimum $E_{\min}$, the linear relationship between the arm energy deviation and the capacitor voltage deviation can be obtained as follows:

$$\Delta E = CNV_{\text{rated}}\Delta V. \tag{14}$$

While in MMC-BESS, the arm energy not only comes from the capacitor but also from the reactor and the battery module. Commonly, the energy ripple generated by the reactor and the battery module cannot be ignored in the calculation because of the large battery current ripple. Since the reactor and battery module are paralleled connected with the capacitor, the battery current has different phase displacement with the capacitor voltage, which indicates that the peak values of the arm energy, capacitor energy, reactor energy, and battery energy ripple are not in the same phase. Therefore, the conventional analysis method cannot derive the relationship between the current deviation, the voltage deviation and the arm energy deviation. Thus, instead of deriving the relationship between different deviations, this article proposes a method to derive the relationship between the amplitude of the arm energy frequency component and the deviation of capacitor voltage and current deviation.

For the simplification of the analysis, the half-bridge submodule is set as the example. Since the main frequency components of the battery current are dc, fundamental and second order, the expression of the submodule battery current is defined as follows:

$$I_L = I_{m0} + I_{m1}\sin(\omega t + \theta_{1\omega}) + I_{m2}\sin(2\omega t + \theta_{2\omega}) \tag{15}$$

where I_{m0}, I_{m1}, and I_{m2} are, respectively, the amplitudes of dc, fundamental ,and second harmonic components of the battery current, which are also the main frequency components of the battery current. According to the characteristic equations of capacity and (15), the expression of capacity voltage can be similarly defined as follows:

$$V_C = V_{m0} + \omega L I_{m1}\cos(\omega t + \theta_{1\omega}) + 2\omega L I_{m2}\cos(2\omega t + \theta_{2\omega}) \tag{16}$$

where V_{m0} is the dc component of capacitor voltage, which equals to the battery voltage V_{bat} in the half-bridge submodule.

In MMC application, the ripple of the capacitor voltage is usually limited within 15% . For the negative effect of the battery current ripple, the battery current should also be limited to a small value. Thus, the dc component is much greater than the other frequency component in both the battery current and the capacitor voltage. Therefore, the product of different ac components' amplitude in the equation can be neglected compared to the product of the dc component and the ac components' amplitude. The expression of the ripple component of the submodule reactor energy can be approximated to

$$\begin{aligned} E_L &= AC\left(\frac{1}{2}LI_L^2\right) = AC\Big(\frac{1}{2}L(I_{m0} + I_{m1}\sin(\omega t + \theta_{1\omega}) \\ &\quad + I_{m2}\sin(2\omega t + \theta_{2\omega}))^2\Big) \\ &\approx L(I_{m0}I_{m1}\sin(\omega t + \theta_{1\omega}) + I_{m0}I_{m2}\sin(2\omega t + \theta_{2\omega})). \end{aligned} \tag{17}$$

Similarly, the expression of the submodule capacitor energy ripple component can be found to be

$$\begin{aligned} E_C &= \text{ac}\left(\frac{1}{2}\text{C}V^2\right) \approx C(\omega L I_{m1}V_{m0}\cos(\omega t + \theta_{1\omega}) \\ &\quad + 2\omega L I_{m2}V_{m0}\cos(2\omega t + \theta_{2\omega})). \end{aligned} \tag{18}$$

The expression of battery energy can be expressed as the integral of the battery output power, which is derived as follows:

$$\begin{aligned} E_{bat} &= \text{ac}\left(\int V_{bat}I_L dt\right) = -V_{bat}\Big(\frac{I_{m1}}{\omega}\cos(\omega t + \theta_{1\omega}) \\ &\quad + \frac{I_{m2}}{2\omega}\cos(2\omega t + \theta_{2\omega})\Big). \end{aligned} \tag{19}$$

The energy of one submodule contains the energy of the battery module, reactor, and capacitor. From (17), (18), and (19), the expression of submodule energy ripple can be expressed as

follows:

$$\begin{aligned} E &= E_L + E_C + E_{bat} = I_{m1}\left(\frac{CL\omega^2 V_{m0} - V_{bat}}{\omega}\cos(\omega t + \theta_{1\omega})\right. \\ &\quad \left. + I_{m0} L \sin(\omega t + \theta_{1\omega})\right) \\ &\quad + I_{m2}\left(\frac{4CL\omega^2 V_{m0} - V_{bat}}{2\omega}\cos(2\omega t + \theta_{2\omega})\right. \\ &\quad \left. + I_{m0} L \sin(2\omega t + \theta_{2\omega})\right) \\ &= K_1 I_{m1}\cos(\omega t + \theta_{1e\omega}) + K_2 I_{m2}\cos(2\omega t + \theta_{2e\omega}) \\ &= E_{1\omega}\cos(\omega t + \theta_{1e\omega}) + E_{2\omega}\cos(2\omega t + \theta_{2e\omega}) \end{aligned} \tag{20}$$

where $E_{1\omega}$ and $E_{2\omega}$ are the amplitude of the fundamental and second submodule energy components. Because K_1 and K_2 are constant in steady state, it can be concluded from (20) that the relationship between the amplitude of the battery current ripple and the submodule energy ripple is proportional.

The proportional relationship between the deviation of energy and the amplitude of the fundamental, second-order component can be obtained by two-dimensional curve-fitting, neglecting the relative phase angle between the fundamental and second-order components [19]. Similarly, according to (20), the relationship between the battery current deviation and the deviation of arm energy can also be given by the following relation:

$$\Delta I_L^2 \approx 4.087 I_{m1}^2 + 7.72 I_{m2}^2 = 4.087\frac{|E_{1\omega}^2|}{K_1} + 7.72\frac{|E_{2\omega}^2|}{K_2} \tag{21}$$

$$\begin{aligned} K_1 &= N^2\left((I_{m0}L)^2 + \left(\frac{LC\omega^2 V_{m0} - V_{bat}}{\omega}\right)^2\right) \\ K_2 &= N^2\left((I_{m0}L)^2 + \left(\frac{4LC\omega^2 V_{m0} - V_{bat}}{2\omega}\right)^2\right) \end{aligned} \tag{22}$$

where $E_{1\omega}$ and $E_{2\omega}$ are the amplitudes of the fundamental and second-order components of the arm energy, which is also the sum of the N submodule energy in the arm. The coefficients 4.087 and 7.72, derived in [19], can be directly utilized in the context of battery current ripple, as the latter constitutes a combination of fundamental and second-order frequency components that are appropriate for the curve-fitting method proposed in [19]. It is obvious from (21) that the relationship between the current deviation and the arm energy frequency component amplitude is quadratic. According to (16) and (21), the analytical expression of the capacitor voltage can also be obtained

$$\begin{aligned} \Delta V &= \sqrt{4.087(\omega L)^2 I_{m1}^2 + 7.72(2\omega L)^2 I_{m2}^2} \\ &= \sqrt{4.087(\omega L)^2\frac{|E_{1\omega}^2|}{K_1} + 7.72(2\omega L)^2\frac{|E_{2\omega}^2|}{K_2}}. \end{aligned} \tag{23}$$

Hence, the analysis of the battery current and capacitor voltage deviation can be converted to the analysis of the arm energy component.

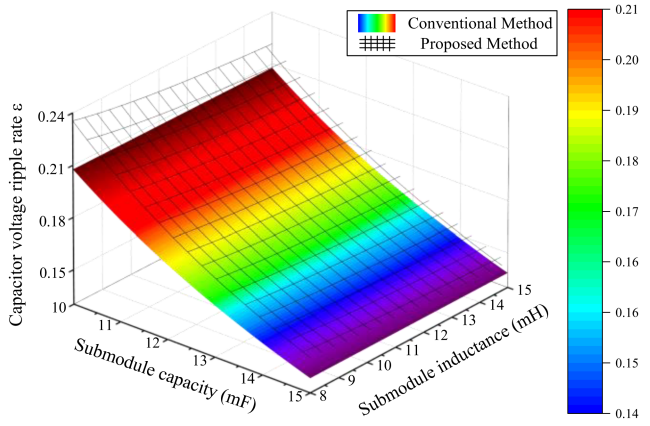

Fig. 3. Comparison of voltage ripple under different inductance and capacitance.

B. Influence of the Reactor and the Battery Module in Capacitor Voltage Deviation

The conventional analysis method assumes that the arm energy ripple completely comes from the capacitors neglecting the effect of the reactor and battery module. Since in (8), (9), and (23), the accurate analytical expression of the capacitor voltage deviation can be obtained, whether neglecting the effect of the reactor and battery module is reasonable or not can be discussed here.

According to the assumption of the conventional analysis method, the voltage deviation is proportional to the energy deviation. Since the frequency components of the arm energy Are fundamental and second order, according to (14), the expression of the capacitor voltage deviation can also be converted to the function of the amplitude of the arm energy frequency components as

$$\begin{aligned} \Delta V &= \Delta E / CNV_{\text{rated}} \\ &= \left(\sqrt{4.087|E_{1\omega}^2| + 7.72|E_{2\omega}^2|}\right)/(CNV_{\text{rated}}). \end{aligned} \tag{24}$$

In contrast, the analytical expression of the capacitor voltage deviation considering the effect of the reactor and battery module is shown in (23) where the different coefficients of the arm energy fundamental and second-order components between (23) and (24) demonstrate the difference of the capacitor voltage ripple rate between with and without the effect of the reactor and the battery module. The difference of the capacitor voltage deviation estimated value between the conventional and proposed analysis method is shown in Fig. 3, where the capacitor voltage ripple rate ε is defined as $\varepsilon = \Delta V/(2V_{\text{rated}})$

In Fig. 3, the estimated value of the proposed method represented by the mesh-grid is greater than the estimated value of the conventional method represented by the color-surface. Since the color-surface also representing the capacitor ripple in MMC is lower compared to that in MMC-BESS, it can be deduced that the inclusion of the battery module and the reactor r results in an increase in the capacitor voltage ripple. It is shown from Fig. 3 that the voltage ripple is also affected by the submodule inductance and the difference of the capacitor voltage

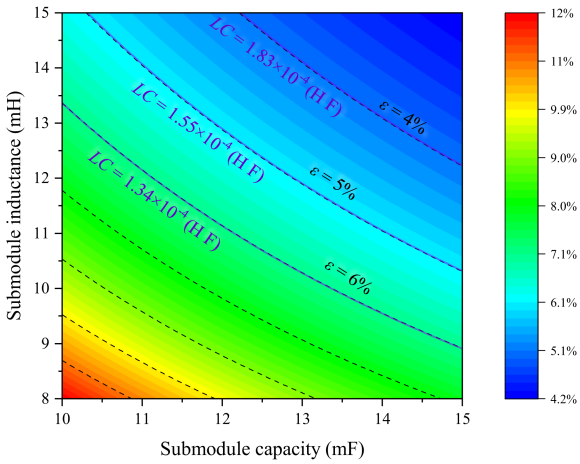

Fig. 4. Comparison of voltage ripple under different inductance and capacitance.

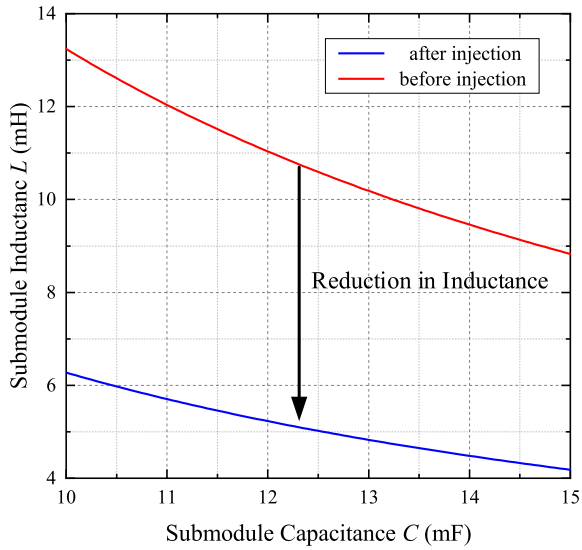

Fig. 5. Comparison of minimum requirement of inductance under different submodule capacitance.

deviation estimated value between different analysis method will significantly increase with the decrease of the capacitance C and the inductance L, but the estimated value difference will become small enough to be ignored when both the inductance and the capacitance are large. As shown in Fig. 4, achieving an error disparity less than 5% between two methods necessitates that the product of the capacitance C and the inductance L exceeds 1.55×10^{-4} HF, which is excessively large and typically unacceptable for practical applications. Therefore, the proposed method is necessary for accurately estimating the capacitor voltage deviation

C. Current Injection Method Optimization

As mentioned before, the current injection method can mitigate both frequency components of energy ripple. Thus, the function of the amplitude of the arm energy can be set as the target function for obtaining the injected current value of optimizing the arm energy ripple suppression effect. To achieve the optimization of the battery current ripple suppression, the analytical expression of the battery current deviation (21) is set as the target function as follows:

$$f(I_{zd},I_{zq})=\Delta I^2=\frac{4.087}{K_1}(E_{1\omega d}^2+E_{1\omega q}^2)+\frac{7.72}{K_2}(E_{2\omega d}^2+E_{2\omega q}^2)$$
$$\frac{\partial f(I_{zd},I_{zq})}{\partial I_{zd}}=0,\quad \frac{\partial f(I_{zd},I_{zq})}{\partial I_{zq}}=0. \tag{25}$$

In order to optimize suppression, the derivative of the target function in I_{zd} and I_{zq} should be zero to get the peak value. The expressions of I_{zd} and I_{zq} can be derived as follows:

$$I_{zd}=\frac{m(0.667mK_2P_{bat}+((0.5m^2-1)K_2-0.475K_1)V_{dc}I_{gd})}{(1.9K_1+m^2K_2)V_{dc}}$$
$$I_{zq}=-\frac{mI_{gq}(0.475K_1+K_2)}{1.9K_1+m^2K_2}. \tag{26}$$

After adopting the current injection method, the battery current deviation will significantly decrease, which means that with the same submodule capacitance, the minimum requirement of inductance for limiting the current ripple within a specified value will be highly decreased. The comparison of the minimum requirement of inductance before and after current injection is shown in Fig. 5.

In Fig. 5, the battery current ripple ratio limitation is set to 50% and the submodule capacity increases from 10 mF to 15 mF. The curve represents the minimum inductance requirement for ensuring that the battery current deviation is within the current ripple ratio limitation. The result shows that the submodule inductance requirement is significantly decreased with the current injection method and the reduction in inductance decreases with the increase of the submodule capacitance.

According to (8), (9), (21), and (26), the full expressions of the current deviation after injecting current can be obtained, which gives us the ability to quantitatively analyze the impact factors of the capacitor voltage and battery current deviation, as well as the ripple suppression effect of the current injection method.

IV. Analytical Expression for Different Influence Factors

This part investigates the influencing factors of current ripple under different operating conditions. According to (25) and (26), there are some parameters that affect the current ripple during operation. First, the MMC-BESS should generate active power according to the requirements of the system operator, thus, the active power reference is an important factor. The second one is the battery output power. If a fault occurs in the battery modules or the battery modules are in a low SOC, MMC-BESS needs to decrease the output power of the battery. Besides, since the modulation index is approximately constant under practical operating conditions, the modulation index is not discussed here.

For simplifying the mathematical analysis of energy ripple here, there are some assumptions.

1) Since the battery energy storage system usually operates at unity power factor, the reactive power reference value is set to zero.
2) For simplicity, the benchmark of the battery output power effect is the proportion of the battery output power and ac-side output power k i.e., $P_{\rm bat} = kP_{\rm ac}$. According to (1), the relationship between k and $P_{\rm dc}$ satisfies that $P_{\rm dc} = -(k+1)P_{\rm ac}$.
3) Compared to other frequency components in arm current, the injected current for SoC balancing is small enough to be neglected.
4) Considering the effect of SoC balancing control strategy, all submodules in the arm are assumed to be well-balanced with the same battery voltage, as well as the six arms.
5) The internal impedance of the battery module is small enough to be neglected compared to the impedance of the submodule capacitor and reactor in fundamental and second-order frequencies.

A. Influence of AC-Side Output Power

First, since the reactive power reference is zero, the q-axis value of the grid current should be zero. Thus, according to (8), (9), and (26), the parameters $E_{2\omega d}$ and $E_{1\omega d}$ are zero. Therefore, in the ripple component of the arm energy only $E_{2\omega q}$ and $E_{1\omega q}$ vary after injecting current, which can be regarded as the benchmarks of the current deviation. For discussing the influence of ac-side output power, the parameters I_{gd} and $P_{\rm bat}$ should be converted to the function of $P_{\rm ac}$. The expression of I_{gd} is shown as follows:

$$I_{gd} = \frac{4P_{\rm ac}}{3mV_{\rm dc}}. \tag{27}$$

Substituting (27) to (8) and (9), the expression of energy frequency components can be simplified to the product of $P_{\rm ac}$ and the constant values K_{p1} and K_{p2} as follows:

$$E_{1q\omega} = K_{p1}P_{\rm ac} \tag{28}$$

$$K_{p1} = \frac{(0.63 + (-0.48 - 0.32k)m^2)K_1 + 8.3 * 10^{-5}km^4K_2}{m\omega(1.9K_1 + m^2K_2)} \tag{29}$$

$$E_{2q\omega} = K_{p2}P_{\rm ac} \tag{30}$$

$$K_{p2} = \frac{(0.175 + (-0.13 - 0.088k)m^2)K_2}{\omega(K_1 + 0.53m^2K_2)}. \tag{31}$$

From (28) and (30), it can be concluded that the energy component is proportional to ac-side output power under the same modulation index m and battery output power proportion k.

As shown in Fig. 6, after injecting current, the relationship between the ac-side output power and the square of the fundamental energy component is a quadratic function, which is similar to the second harmonic one. Therefore, as the absolute value of the ac-side output power increases, the energy ripple will increase after adopting the current injection method. Fig. 6 shows the difference of $E_{1\omega q}$ before and after injection under different ac-side output power and different battery output power, where the mesh grid representing the energy component before injecting current is significantly greater than the colored-surface representing the energy component after injecting current, which indicates that the current injection method can not only mitigate the deviation of the energy components, but also effectively reduce the derivative of the energy component in the axis of the ac-side output power.

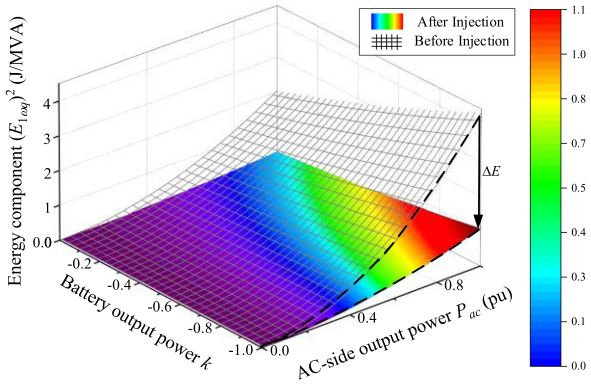

Fig. 6. Comparison of energy component before and after injecting current under different AC-side output $P_{\rm ac}$.

B. Influence of Output Power Proportion Between Battery and DC-Bus

Substituting (26) to (8) and (9), the expressions of $E_{2\omega q}$ and $E_{1\omega q}$ can also be converted to the function of the battery output power proportion, then the expression can be simplified to the first order polynomial as follows:

$$E_{1q\omega} = K_{k1} + K_{k2}k \tag{32}$$

$$\begin{cases} K_{k1} = \frac{(0.633-0.475m^2)K_1P_{\rm ac}}{(1.9K_1+m^2K_2)m\omega} \\ K_{k2} = \frac{(-0.317m^2K_1+8.3*10^{-5}m^4K_2)P_{\rm ac}}{(1.9K_1+m^2K_2)m\omega} \end{cases} \tag{33}$$

$$E_{2q\omega} = K_{k3} + K_{k4}k \tag{34}$$

$$\begin{cases} K_{k3} = \frac{(0.175-0.132m^2)K_2P_{\rm ac}}{(K_1+0.526m^2K_2)\omega} \\ K_{k4} = -\frac{0.0878m^2P_{\rm ac}}{(K_1+0.526m^2K_2)\omega}. \end{cases} \tag{35}$$

The difference between $E_{2\omega q}$ and $E_{1\omega q}$ in different battery output power is shown in Fig. 7. The result indicates that in the same ac-side output power, with the decreasing of battery output power, the energy ripple declines. It is worth noting that the benchmark $E_{1\omega q}$ is always larger than 0 under different modulation index m and output power proportion k, which ensures that the negative correlation between k and the square of the energy component always exists in the work range of MMC-BESS.

As shown in Fig. 7, the mesh grid representing the energy component before injecting current is higher than the colored surface representing the energy component after injecting current and the difference between the mesh grid and the colored surface does not increase significantly with the increasement

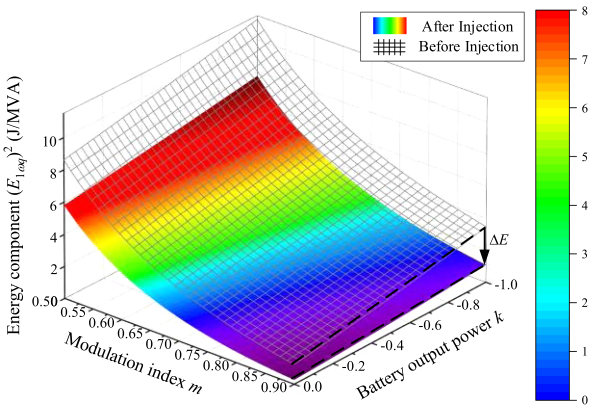

Fig. 7. Comparison of energy component before and after injecting current under different battery output power.

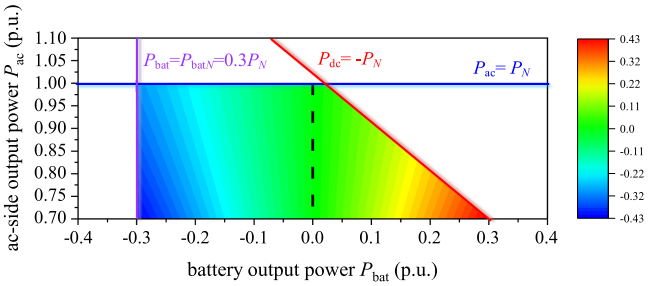

Fig. 8. Output power proportion k under different battery output power and AC-side output power.

of the battery output power, which indicates that the mitigating effect of the current injection method is insensitive to the battery output power proportion.

According to (1) and each port's output power should be less than the rated power of MMC-BESS P_N, the limitation can be mathematically expressed as

$$\begin{cases} |P_{\rm dc}| = |P_{bat} + P_{\rm ac}| \le P_N \\ |P_{bat}| \le P_{batN} \\ |P_{\rm ac}| \le P_N. \end{cases} \tag{36}$$

Fig. 8 illustrates the constraints on the three ports in the MMC-BESS, as derived from (36). The red line denotes the constraint on the dc-side output power ($P_{\rm dc} = -(P_{\rm bat}+P_{\rm ac}) \le P_N$), the blue line represents the constraint on the ac-side output power ($P_{\rm ac} \le P_N$), and the purple line signifies the constraint on the battery output power ($P_{\rm bat} \le P_{\rm bat\,}{}_N$). As the Fig. 8 shown, the range of the battery output proportion k can be extended with the decrease of the ac-side output power $P_{\rm ac}$ decrease. The comparison between the energy component under different ac-side output $P_{\rm ac}$ with the limitation of k are shown in Fig. 9.

In Fig. 9, the ac-side output power is exemplified by values of 8 MW (1.0 p.u.), 6.8 MW (0.85 p.u.), and 5.6 MW (0.7 p.u.), with the battery output power $P_{\rm bat}$ constrained to $0.3P_{\rm N}$. It can be deduced that as the ac-side output power decreases, the range of the battery output power proportion k increases, while both the maximum and minimum values of the energy component $E_{1\omega\,q}$ diminish accordingly.

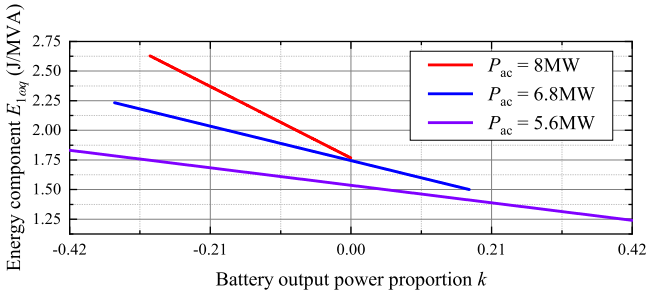

Fig. 9. Comparison of energy component under different AC-side output $P_{\rm ac}$ with the limitation of k.

C. Conclusion of Impact Factors

Based on the abovementioned analysis, the energy ripple suppression effect of the injection method under different impact factors is compared to investigate the effect of the impact factors. Some important conclusions can be drawn from the analysis as follows.

1) Different energy frequency components have the same variation direction with or without current injection under different impact factors.
2) The ac-side output power and the deviation of energy have a positive correlation. The proportion of battery output power k and the energy deviation have a negative correlation.
3) The mitigating effect of injecting current is sensitive to the ac-side output power, but insensitive to the battery output power proportion.

D. Control Strategy

The MMC-BESS controller consists of three parts: 1) the power controller, 2) the current controller, and 3) the gate signal generator, as shown in Fig. 10. Through the ac-side power controller, the active and reactive output power reference P_{ref} and Q_{ref}, respectively, determine the d-axis and q-axis component of the ac-side output current i_d and i_q. Besides, the battery power controller generates the reference of the dc component of the circulating current i_{cirj} to control the dc-side output power $P_{\rm dc}$, thereby achieving the control of battery output power $P_{\rm bat}$. In MMC application, the circulating current controller is used to suppress the negative-sequence second-order frequency component of circulating current i_{cirj} to zero [21]. In this article, the reference values for the d-axis and q-axis components of the negative-sequence second-order frequency component in the circulating current are designated as i_{zd} and i_{zq} based on (26) to optimize the submodule battery current ripple suppression effect. The gate signals generator is utilized to generate gate signals for each power switch within the submodule, which includes carrier-wave shifting pulsewidth modulation [22]. To balance the SoC of the battery modules in different submodules, The SoC balancing control is integrated to three layers of the control strategy, including the phase SoC balancing, arm SoC balancing, and the submodule SoC balancing [23].

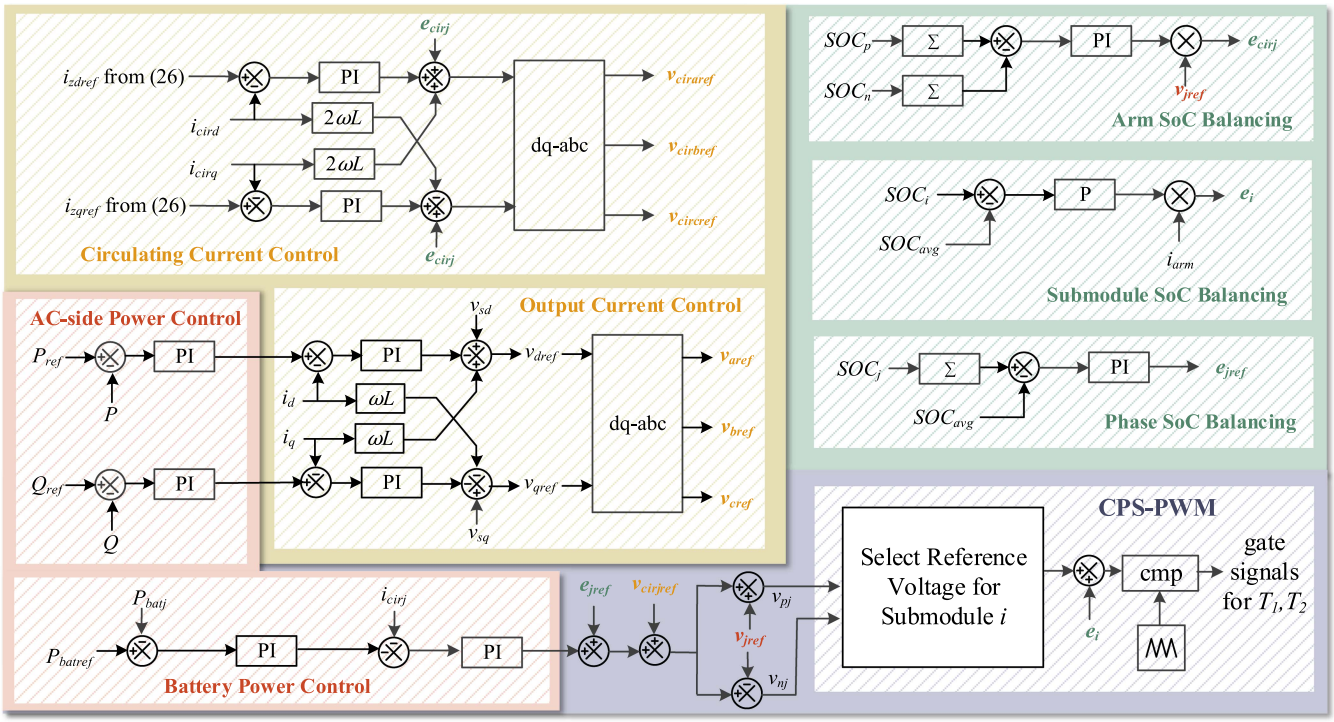

Fig. 10. Block diagram of control strategy.

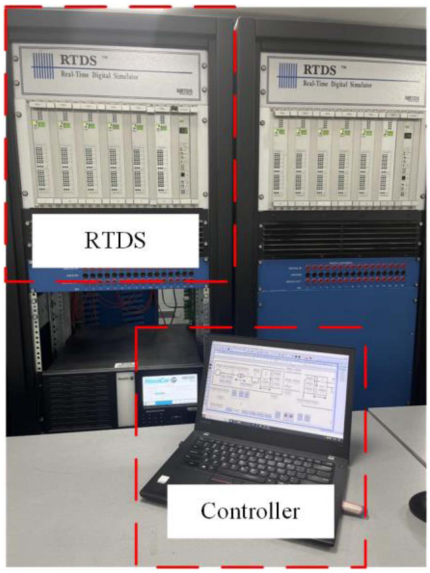

Fig. 11. Photograph of the simulation platform.

TABLE I
PARAMETERS OF REAL TIME SIMULATION

Parameter	Rating
Dc-bus voltage V_{dc}	12 kV
Modulation index m	0.85
Number of SM per arm N	12
Submodule capacity C	15 mF
Submodule reactance L_s	8.8 mH
Battery voltage V_{bat}	998 V
Grid frequency f	50 Hz
Arm Inductance L_{arm}	4.5 mH

V. VALIDATION

A. Comparison of the Real Time Simulation Results of Before and After Current Injection

An MMC-BESS model within the real time digital simulation system (RTDS) (as shown in Fig. 11) is built to verify the analysis of the capacitor voltage deviation, battery current deviation, and the variation of the energy components under different operating conditions. The main parameters are shown in Table I. Fig. 12 shows the comparison of the battery current, capacitor voltage, and arm current before and after adopting the current injection method. The real time simulation is performed for the case when the MMC-BESS delivers the active power value $P_{\rm ac} = +8$ MW and the battery output power proportion $k = -0.3$.

In Fig. 12, the MMC-BESS is initially operating without injecting current. Before injecting the current, the deviations of the battery current and the capacitor voltage are 0.32 kV and 16 A, respectively. At $t = 1.0$ s, the current injection method is adopted and the second harmonic is injected into the arm current. After implementing the current injection method, the amplitude of the capacitor voltage ripple and the battery current ripple is suppressed about 34% and 41% , while the arm current rms increases about 48% . Given the necessity for high current-rating semiconductor devices due to the extremely high peak arm current following current injection, the current limitation method [21] can be employed to mitigate arm current, while ensuring optimized current ripple suppression under the constraint of injected current. The arm voltage, output voltage, and output current exhibit virtually no discernible difference before and

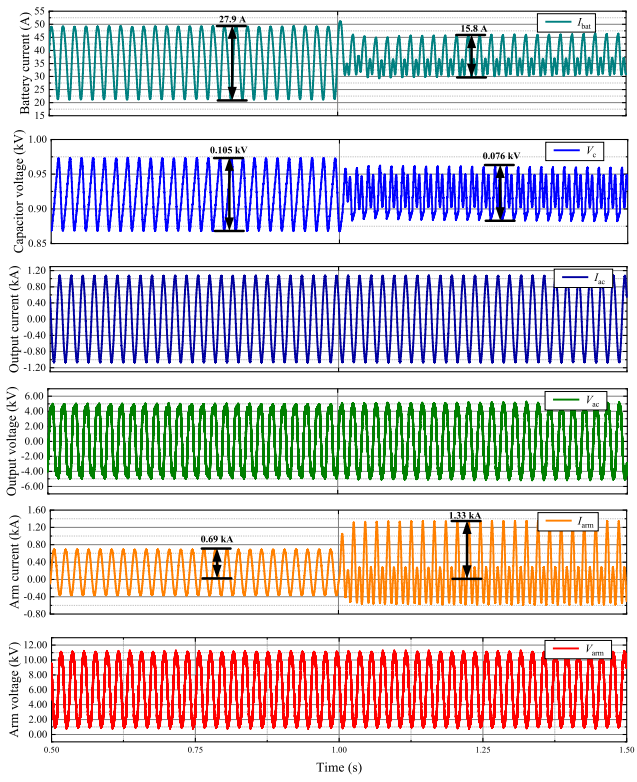

Fig. 12. Comparison of capacitor voltage and battery current after and before injecting current.

TABLE II
COMPARISON OF THE SIMULATION RESULTS

Mode	Battery current deviation ΔI	Injection Value I_z
SHES	22.1 A	0.22 kA
UOE	19.9 A	0.42 kA
Proposed Method	15.6 A	0.65 kA

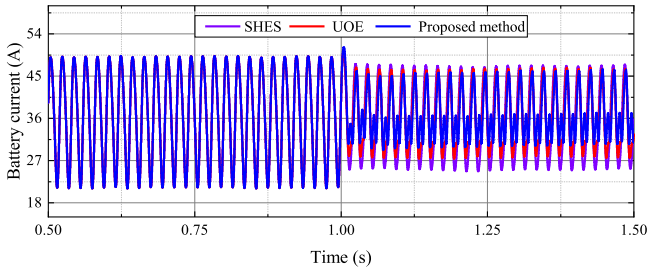

Fig. 13. Comparison of battery current under different injection method.

after current injection. The simulation results reveal that the optimized current injection method has good performance in suppressing the ripple of the battery current without affecting the output current and voltage but requires semiconductor devices having higher current ratings.

As illustrated in Table II and Fig. 13, when compared to the second-harmonic energy ripple suppression (SHES) method [18] and the unconstrained optimization of energy deviation (UOE) approach [19], the proposed method exhibits a superior effect in suppressing battery current ripple but requires a higher injection current value. Since both SHES and UOE methods target suppressing the capacitor voltage ripple and ignoring the effect of the reactor and battery module, the proposed method exhibits better performance in mitigating battery current deviation.

B. Validation of the Real Time Simulation Results of Different Operating Conditions

For validating the accuracy of the analysis method mentioned in Sections III and IV, different operating conditions are set. The calculation and simulation results are shown in Fig. 14.

In Fig. 14(a), the ac-side output power increases from 0 MW to +8 MW under the battery output power proportion $k = -0.3$. The energy components increase with the increase of the ac-side output power $P_{\rm ac}$ and the simulation results show a proportional relationship between the energy components $E_{1\omega q}$, $E_{2\omega q}$ and the ac-side output power $P_{\rm ac}$, and the proportion of the fundamental and second-harmonic energy components is constant.

In Fig. 14(b), the battery output power proportion k increases from -0.3 to 0, i.e., the battery output power decreases from 1.0 p.u. to 0.0 p.u., where $P_{\rm ac} = +8$ MW. The simulation results show that both arm energy in the fundamental component $E_{1\omega q}$ and second-order harmonic component $E_{2\omega q}$ decrease with the increase of the battery output power proportion k and a good proportional relationship between the energy and the ac-side output power $P_{\rm ac}$. The decreasing degree of the fundamental component is much greater than the one in the second harmonic since the $I_{\rm dc}$ item is significantly affected by the battery output power. In Fig. 15, the lines representing the energy components under $P_{\rm ac} = +1.0$ p.u. are lower compared to the lines in Fig. 14(b) depicting the energy components under $P_{\rm ac} = +0.85$ p.u. and the maximum and minimum values of both energy components diminish. Furthermore, the expressions for both energy components within the ranges of $k>0$ and $k<0$ can be described by the same equation.

In Fig. 14(c) and (d), the ac-side output power $P_{\rm ac}$ is increasing from 0 to +8 MW and the battery output power proportion $k = -0.3$. The battery current deviation and capacitor voltage deviation increase with the increase of $P_{\rm ac}$, which completely meets the theoretical derivation in (21) and (23) that the battery deviation and the capacitor voltage deviation have a proportional relationship to the energy component. The above comparison results reveal a good degree of matching between the calculation and simulation, justifying the high accuracy of the analytical expressions in Sections III and IV. Conversely, the estimated values of the capacitor voltage ripple based on the conventional method display notable discrepancies when compared to the simulation results.

In Fig. 16, the ac-side output power $P_{\rm ac}$ is increasing from 0.47 to 8 MW and the battery output power $P_{\rm bat}$ is constant from $t = 0.5$ to $t = 2$ s. It can be observed that the injected current value increase with the increase of the ac-side output power $P_{\rm ac}$. Similarly, the injected current values also decrease with the reduction of the battery output power $P_{\rm bat}$ and the ac-side output power $P_{\rm ac}$ is constant from $t = 2$ s to $t = 3.5$ s. These observations validate that the proposed method can adjust the

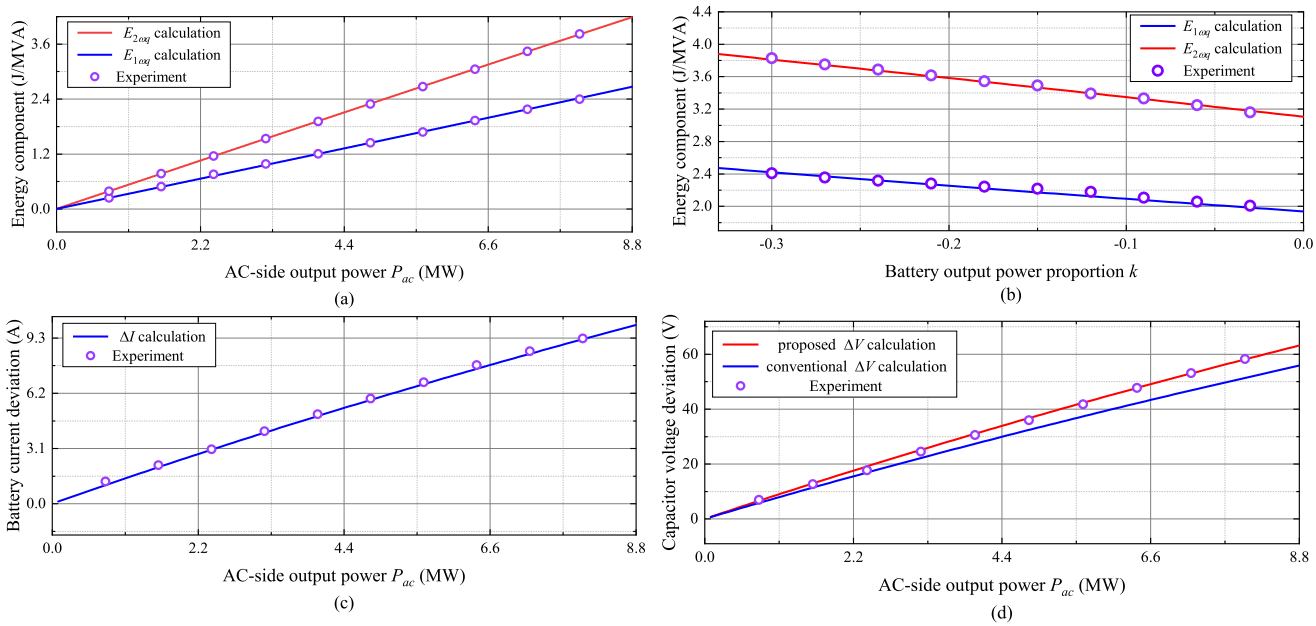

Fig. 14. Comparison of calculation and simulation results of different energy ripple factors. (a) Comparison of energy component under different AC-side output power, (b) comparison of energy component under different battery output power, (c) comparison of battery current ripple under different AC-side output power, and (d) comparison of capacitor voltage ripple under different AC-side output power.

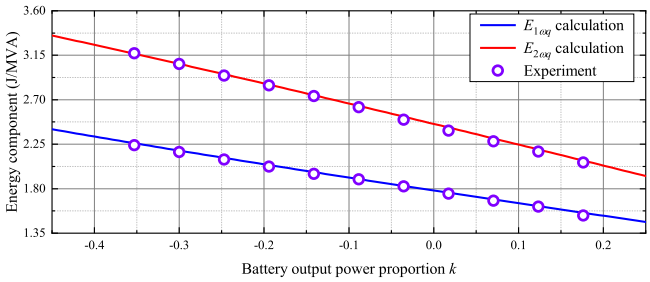

Fig. 15. Comparison of calculation and simulation results under different the output power proportion k at $P_{\mathrm{ac}} = 0.85$ p.u.

injected current values to achieve an optimized battery current suppression effect under varying operational conditions.

C. Validation of the Positive Effect of the Current Injection Method in Improving Battery Life

A downscale battery experimental platform is built to verify the positive effect of decreasing the deviation of battery current as shown in Fig. 17. In comparison to the battery current before and after injecting current, two batteries were cycled one charge/discharge cycle with different current, which is equivalent to the battery current before and after injecting current in RTDS simulation under rated ac-side output power $P_{\mathrm{ac}} = +8$ MW and battery output power proportion $k = -0.3$. The main parameter of battery experiment is shown in Table III.

Fig. 18 shows the experimental results of battery capacity changes when the current injection method is adopted or not. For unifying the charge current between different batteries, the charge current is usually given by C-rate, which is the current that can totally discharge the battery in 1 h. The red and blue curves, respectively, represent the battery capacity fading under

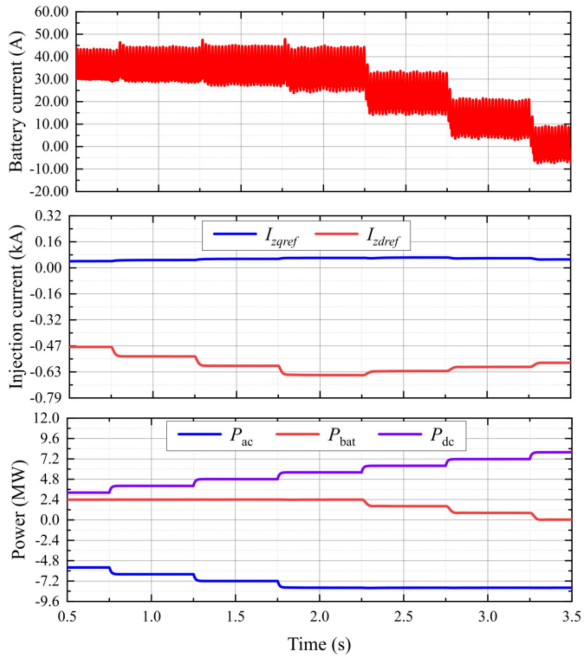

Fig. 16. Comparison of injection current under different ac-side output power P_{ac} and battery output power P_{bat}.

TABLE III
PARAMETERS OF BATTERY CYCLE EXPERIMENT

Parameter	Rating
Battery type	$LiFePO_4$
Nominal capacity	156 Ah
Charge cut-off voltage	3.65 V
Discharge cut-off voltage	3.0 V
Charge current dc component	1C
Charge current ac component	0.25C/0.5C
Room temperature	25°C

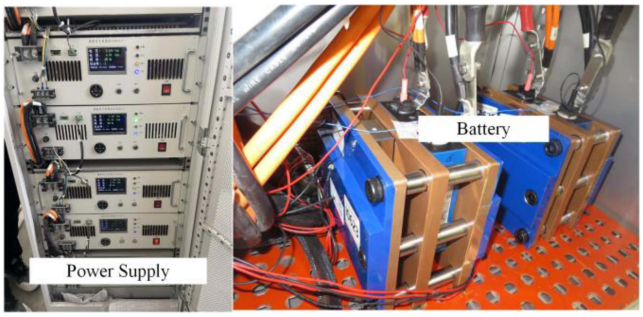

Fig. 17. Photograph of battery experimental platform.

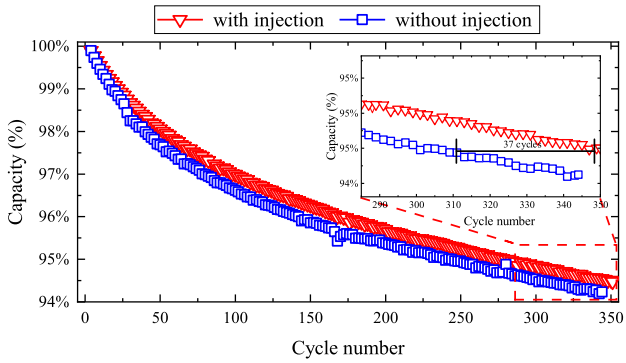

Fig. 18. Comparison of the battery capacity under different discharging current.

the battery current ripple amplitude is about 0.25 C and 0.5 C. It is evident that the red curve lies above the blue curve, indicating that the battery employing the current injection method exhibits a slower capacity fade rate. Furthermore, the battery with current injection maintains 95% of its capacity for 348 cycles, representing an 11% increase compared to the battery without current injection. The reason for this is that the reduction in conduction loss due to ohmic resistance, reflecting the lithium battery degradation [24], is attributed to the decrease in harmonic amplitude following current injection.

VI. Conclusion

This article proposes an analysis method for the battery current and capacitor voltage ripple of MMC-BESS and an optimization method to mitigate the ripple by injecting current. The analysis of the ripple of the current and voltage in one single submodule can be converted into the analysis of the arm energy component. The effect of the reactor and the battery module on the voltage and current ripple is investigated. The incorporation of the battery module and the reactor results in an increase in the capacitor voltage ripple and invalidates the proportional relationship between the arm energy deviation and the capacitor deviation. The analytical expression of the capacitor voltage and battery current deviation is derived to obtain the optimized injected current value, giving the ability to quantitatively analyze the effect of the current injection method under different operating conditions.

The influence of ac-side output power and battery output power is analyzed, which shows that the decrease of ac-side and battery output power can help suppress the battery current ripple. The effect of the current injection method under different ac-side and battery output power is investigated and it can be seen that the mitigating effect of the current injection is sensitive to the ac-side output power, while being insensitive to the battery output power.

The experiment results have fully validated the analytical expression of the voltage and current deviation and the analysis of the arm energy component variation, as well as the effectiveness of the current injection method for mitigating current and voltage ripple. The results also verify that with the current injection method, the capacity fading speed of the battery will be significantly decreased.

References

[1] J. Fang, Y. Tang, H. Li, and X. Li, "A battery/ultracapacitor hybrid energy storage system for implementing the power management of virtual synchronous generators," *IEEE Trans. Power Electron.*, vol. 33, no. 4, pp. 2820–2824, Apr. 2018.

[2] X. Meng, J. Liu, and Z. Liu, "A generalized droop control for grid-supporting inverter based on comparison between traditional droop control and virtual synchronous generator control," *IEEE Trans. Power Electron.*, vol. 34, no. 6, pp. 5416–5438, Jun. 2019.

[3] X. Wang, F. Blaabjerg, and W. Wu, "Modeling and analysis of harmonic stability in an AC power-electronics-based power system," *IEEE Trans. Power Electron.*, vol. 29, no. 12, pp. 6421–6432, Dec. 2014.

[4] G. S. Wang et al., "A review of power electronics for grid connection of utility-scale battery energy storage systems," *IEEE Trans. Sustain. Energy*, vol. 7, no. 4, pp. 1778–1790, Oct. 2016.

[5] H. Xue, J. He, Y. Ren, and P. Guo, "Seamless fault-tolerant control for cascaded H-bridge converters based battery energy storage system," *IEEE Trans. Ind. Electron.*, vol. 70, no. 4, pp. 3803–3813, Apr. 2023.

[6] G. Liang et al., "Unbalanced active power distribution of cascaded multilevel converter-based battery energy storage systems gobble," *IEEE Trans. Ind. Electron.*, vol. 69, no. 12, pp. 13022–13032, Dec. 2022.

[7] G. Liang et al., "A constrained intersubmodule state-of-charge balancing method for battery energy storage systems based on the cascaded H-bridge converter," *IEEE Trans. Power Electron.*, vol. 37, no. 10, pp. 12669–12678, Oct. 2022.

[8] M. Vasiladiotis and A. Rufer, "Analysis and control of modular multilevel converters with integrated battery energy storage," *IEEE Trans. Power Electron.*, vol. 30, no. 1, pp. 163–175, Jan. 2015.

[9] G. Liang et al., "Analytical derivation of intersubmodule active power disparity limits in modular multilevel converter-based battery energy Storage systems," *IEEE Trans. Power Electron.*, vol. 36, no. 3, pp. 2864–2874, Mar. 2021.

[10] J. M. L. Fonseca, S. R. P. Reddy, K. Rajashekara, and K. R. R. Potti, "Reduced capacitor energy requirements in battery energy storage systems based on modular multilevel converters," *IEEE Trans. Ind. Appl.*, vol. 58, no. 6, pp. 7608–7619, Nov./Dec. 2022.

[11] A. J. Ruddell et al., "Analysis of battery current microcycles in autonomous renewable energy systems," *J. Power Sources*, vol. 112, no. 2, pp. 531–546, Nov. 2002.

[12] J. B. Axén et al., "Short-term impact of AC harmonics on aging of NiMH batteries for grid storage applications," *Materials*, vol. 14, no. 5, Mar. 2021, Art. no. 8.

[13] A. Ghassemi, A. F. Hollenkamp, P. C. Banerjee, and B. Bahrani, "Impact of high-amplitude alternating current on LiFePO4 battery life performance: Investigation of AC-preheating and microcycling effects," *Appl. Energy*, vol. 314, May 2022, Art. no. 118940.

[14] Z. Ma et al., "Multilayer SOH equalization scheme for MMC battery energy storage system," *IEEE Trans. Power Electron.*, vol. 35, no. 12, pp. 13514–13527, Dec. 2020.

[15] M. Huang, Z. Kang, W. Li, J. Zou, X. Ma, and J. Li, "Modified modular multilevel converter with third-order harmonic voltage injection to reduce submodule capacitor voltage ripples," *IEEE Trans. Power Electron.*, vol. 36, no. 6, pp. 7074–7086, Jun. 2021.

[16] M. Vasiladiotis, N. Cherix, and A. Rufer, "Accurate capacitor voltage ripple estimation and current control considerations for grid-connected

modular multilevel converters," *IEEE Trans. Power Electron.*, vol. 29, no. 9, pp. 4568–4579, Sep. 2014.
[17] Z. Li, Q. Song, S. Xu, B. Zhao, Z. Yu, and R. Zeng, "Analysis and optimization of energy variations in MMCs with variable DC voltages," *IEEE Trans. Power Electron.*, vol. 37, no. 12, pp. 14562–14574, Dec. 2022.
[18] Z. Li, R. Lizana, S. M. Lukic, A. V. Peterchev, and S. M. Goetz, "Current injection methods for ripple-Current suppression in delta-configured split-battery energy storage," *IEEE Trans. Power Electron.*, vol. 34, no. 8, pp. 7411–7421, Aug. 2019.
[19] D. Samajdar and T. Bhattacharya, "Capacitor voltage ripple optimization in modular multilevel converter using synchronous reference frame energy ripple controller," *IEEE Trans. Power Electron.*, vol. 37, no. 7, pp. 7883–7895, Jul. 2022.
[20] M. M. C. Merlin and T. C. Green, "Cell capacitor sizing in multilevel converters: Cases of the modular multilevel converter and alternate arm converter," *IET Power Electron*, vol. 8, no. 3, pp. 350–360, Mar. 2015.
[21] S. Debnath, J. Qin, B. Bahrani, M. Saeedifard, and P. Barbosa, "Operation, control, and applications of the Modular Multilevel converter: A review," *IEEE Trans. Power Electron.*, vol. 30, no. 1, pp. 37–53, Jan. 2015.
[22] B. Li, R. Yang, D. Xu, G. Wang, W. Wang, and D. Xu, "Analysis of the phase-shifted carrier modulation for modular multilevel converters," *IEEE Trans. Power Electron.*, vol. 30, no. 1, pp. 297–310, Jan. 2015.
[23] S. Ali et al., "Prospective submodule topologies for MMC-BESS and its control analysis with HBSM," *Electronics*, vol. 12, no. 1, Jan. 2023, Art. no. 1.
[24] Y. Yang, W. X. Hu, Y. F. Peng, and Y. M. Wei, "Application of electrochemical impedance spectroscopy to degradation and aging research of lithium-ion batteries," *J. Phys. Chem. C*, vol. 127, no. 9, pp. 4465–4495, Mar. 2023.

Yongzheng Yu received the B.S. degree in information system from north china electric power university, china, in 2021. He is currently working toward the M.S. degree in electrical engineering.

His research interest includes the grid-integration of energy storage systems with multilevel power converters.

Xiaolei Cheng received the B.S. and M.S. degrees in electrical engineering from Hebei University of Technology, Hebei, China, in 2015 and 2018, respectively.

Since 2018, he has been with Xuji Group Corporation, Xuchang, China. His research interests include high voltage direct current system, flexible direct current transmission, and offshore wind energy flexible direct current transmission.

Junfang Hao received the B.S. and M.S. degrees in electrical engineering from Taiyuan University of Technology, Shangxi, China, in 1997 and 2002, respectively.

Since 2002, he has been with Xuji Group Corporation, Xuchang, China. His research interests include control and protection system of ultrahigh voltage direct current transmission.

Xiaotian Yuan (Member, IEEE) received the B.S. and Ph.D. degrees in electrical engineering from Xi'an Jiaotong University, Xi'an, China, in 2017 and 2023, respectively.

From 2021 to 2022, he was a China Scholarship Council-funded visiting Ph.D. student with Nanyang Technological University, Singapore. He is currently a Senior Engineer with Contemporary Amperex Future Energy Research Institute, Shanghai, China. His research interests include power system stability and control, grid-forming controls, subsynchronous oscillation analysis, and mitigation.

Qiufeng Shang received the B.S. degree in electrical engineering from the University of Electronic Science and Technology of China, Chengdu, China, in 1990, and the Ph.D. degree in electrical engineering from North China Electric Power University, Baoding, China, in 2005.

She is currently a Full Professor with the School of Electronic and Communication Engineering, North China Electric Power University. She has authored and coauthored more than 80 papers in international and Chinese journals and authorized more than ten Chinese patents. Her research interests include nonlinear fiber optics, distributed optical fiber sensing, fiber Bragg grating sensing, photoelectric detection, and applications of electronic technology.

Ying Yang (Member, IEEE) was born in Hebei province, China, in 1981. She received the B.S. degree in environmental engineering from Tsinghua University, Beijing, China, in 2003, and the Ph.D. degree in electrical engineering from Tsinghua University, Beijing, China, in 2008.

In 2010, she was an Assistant Professor with the Faculty of Electrical Engineering, Tsinghua University, where she became an Associate Professor, in 2011. Her main research interests include insulating materials, next generation of energy devices, and energy storage applications.